Journal of Materials Chemistry A

Accepted Manuscript

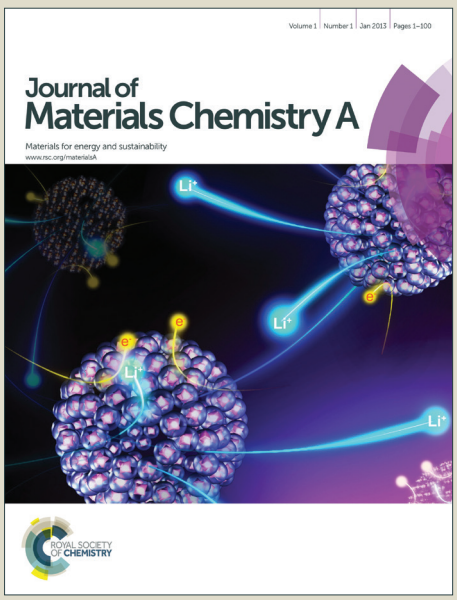

ROYAL SOCIETY OF CHEMISTRY

www.rsc.org/materialsA

Journal of Materials Chemistry A

RSCPublishing

ARTICLE

Synthesis of $LiMn_{0.75}Fe_{0.25}PO_4$/C microspheres using a microwave-assisted process with a complexing agent for high-rate lithium ion batteries

Cite this: DOI: 10.1039/x0xx00000x

Myeong-Seong Kim[a], Jong-Pil Jegal[a], Kwang Chul Roh[*b] and Kwang-Bum Kim[*a]

Received 00th January 2012,
Accepted 00th January 2012

DOI: 10.1039/x0xx00000x

www.rsc.org/

$LiMn_{0.75}Fe_{0.25}PO_4$/C microspheres were synthesized using a microwave-assisted process with a complexing agent. In this process, it was found that the various states of the complexing agent for different pH of the precursor solution have significant effects on the obtained micro spherical morphology. Furthermore, the concentration of antisite defects in the samples was also found to be affected by the pH of the precursor. The prepared secondary spheres have a high tap density of 1.3 g cm^{-3} and deliver a reversible capacity of 163 mAh g^{-1} at a 0.05 C-rate. Furthermore, remarkable rate capability is obtained, with 57% capacity retention at a 60 C-rate, as well as excellent cyclability, with 99.3% capacity retention after 100 cycles at 1 C-rate.

Introduction

Olivine-structured $LiFePO_4$ has been considered a promising cathode material for lithium ion batteries (LIBs) because of its low cost, high theoretical capacity, environmental friendliness, and thermal stability.[1, 2] However, $LiFePO_4$ has a lower energy density than conventional cathode materials because of its low operation voltage (3.5 V vs. Li/Li^+). Therefore, $LiMnPO_4$, which has a higher operation voltage (4.1 V vs. Li/Li^+), is currently considered a more appropriate cathode material than $LiFePO_4$.[3-6] Up to now, the use of $LiMnPO_4$ in electrochemical applications has been limited by its extremely poor electronic conductivity ($<10^{-12}$ S cm^{-1}), low lithium diffusion rate ($<10^{-16}$-10^{-14} cm^2 s^{-1}), Jahn-Teller distortion during the charge-discharge process, and unstable delithiated phase.[7-12] Among these problems, a key factor preventing more widespread utilization of $LiMnPO_4$ is its very low Li^+ diffusion rate at the mismatched $MnPO_4$-$LiMnPO_4$ interface.[8]

In order to resolve these problems with $LiMnPO_4$, the Fe-doped $LiMn_{1-x}Fe_xPO_4$ solid solution system has been suggested.[6, 7, 13-16] Previous research on $LiMn_{1-x}Fe_xPO_4$ has focused on the synthesis of nanoparticles to improve the Li^+ diffusion in the $LiMn_{1-x}Fe_xPO_4$ solid solution system. This approach has led to good cell performance, including high specific capacities and rate capabilities.[6, 17-19] However, the nanoparticles have a low tap density, which limits the volumetric energy density.[20, 21] For example, nanoparticles have tap densities of 0.3–0.8 g cm^{-3}, whereas the conventional oxide electrode material $LiCoO_2$ has a tap density of 2.6 g cm^{-3}. In addition, the extended contact area between the nanoparticles and the electrolyte leads to undesirable side reactions, poor thermal stability, and poor cycling stability.[21]

In contrast with nanoparticles, $LiMn_{1-x}Fe_xPO_4$ microspheres composed of nanosized primary particles can provide a high tap density, high volumetric energy density, and good cyclability. A few studies have focused on the synthesis of microspheres to improve the tap density and electrochemical properties of the material.[22-27] Sun *et al.* used a co-precipitation technique to fabricate $LiMn_{0.85}Fe_{0.15}PO_4$/C microspheres with a high volumetric capacity.[24] Liu *et al.* used a spray-drying technique to fabricate $LiMn_{0.4}Fe_{0.6}PO_4$/C microspheres with a high specific capacity and good rate capability.[26] However, the previously reported methods have been time-consuming, complex two-step or multistep processes involving the use of a microsized spherical $MPO_4 \bullet H_2O$ (M=Fe, Mn) precursor or spray-drying of presynthesized nanoparticles. In addition, microsized $LiMn_{1-x}Fe_xPO_4$ particles have limited specific capacitance and rate capability, since their Li^+ diffusion path is longer than that of the nanoparticles, which leads to electrochemical isolation of the inner parts of the particles.[23] Therefore, a simple and facile synthesis of micro spherical $LiMn_{1-x}Fe_xPO_4$ particles with a high tap density and superior rate capability is highly desirable.

Herein, we report a microwave-assisted synthesis of $LiMn_{1-x}Fe_xPO_4$/C (x = 0.25) microspheres with a complexing agent to achieve both a high tap density and superior rate capability. In particular, we control the pH of the precursor solution to fabricate $LiMn_{1-x}Fe_xPO_4$ microspheres with a low concentration of antisite defects. Spherical $LiMn_{1-x}Fe_xPO_4$ secondary particles were finally obtained under weak acidic conditions. The

morphology and structure of obtained microspheres were characterized by means of field emission scanning electron microscopy (FE-SEM), transmission electron microscopy (TEM), and X-ray diffraction (XRD) analysis. The antisite defect concentration was analyzed by performing Fourier transform infrared spectroscopy (FTIR) measurements. Finally, it is found that the $LiMn_{1-x}Fe_xPO_4$ microspheres prepared in this study exhibit a high tap density, high specific capacity, excellent rate performance, and superior cycling stability as cathode materials for LIBs.

Experimental

Materials synthesis

The $LiMn_{0.75}Fe_{0.25}PO_4$ microspheres were synthesized with a complexing agent using a simple and facile microwave-assisted process. To fabricate $LiMn_{1-x}Fe_xPO_4$ microspheres with low concentrations of antisite defects, the pH of the precursor was controlled by using a mixed P source consisting of H_3PO_4 (Aldrich) and $(NH_4)H_2PO_4$ (Aldrich). The $LiOH \cdot H_2O$ (Aldrich) aqueous solution (1.5 M) and $xH_3PO_4 + (1\text{-}x)(NH_4)H_2PO_4$ ($0 \leq x \leq 1$) aqueous solution (0.5 M) were mixed by strong magnetic stirring at room temperature for a few minutes. Then, $MnSO_4 \cdot H_2O$ (Aldrich) aqueous solution (0.5 M), $FeSO_4 \cdot 7H_2O$ (Aldrich) aqueous solution (0.5 M), and citric acid (Junsei Chemical) aqueous solution (1 M) were added into the above mixture. The citric acid used as the complexing agent prohibits the oxidation of Mn^{+2} and Fe^{2+} to Mn^{3+} and Fe^{3+}. The Li:(Mn+Fe):P molar ratio in the precursor was set to 3:1:1. The detailed compositions of the different precursor solutions used are listed in Table S1. The mixed solution was then loaded into a 100 ml Teflon vessel, which was then sealed and placed in the microwave reaction system (MARS-5, CEM Corporation). The mixture was rapidly heated to 200 °C at a power of 200 W. During the synthesis, the solution temperature was maintained at 200 °C for 15 min with rotation and magnetic stirring. After the reaction, the vessel was cooled down to room temperature, and the final product was repeatedly washed with distilled water and acetone by centrifugation and then dried at 60 °C for 6 h in a convection oven. To provide a uniform carbon coating on the surfaces of the $LiMn_{0.75}Fe_{0.25}PO_4$ microspheres, they were mixed with sucrose in a weight ratio of 9:1. The mixture was then sintered at 650 °C for 3 hours under an Ar/H_2 (95/5 vol%) atmosphere with a heating rate of 5 °C min^{-1}.

Materials characterization

The crystalline phase of the samples was characterized by performing powder XRD (Dmax 2200, Rigaku) measurements with Cu-Kα radiation (λ = 1.5406 Å). The morphologies of the samples were observed by performing FE-SEM (JSM-7001F, JEOL Ltd.), TEM (CM 200, Philips), and high resolution TEM (HRTEM, JEM 2100F, JEOL Ltd.). The cross-sectional TEM specimens were prepared by slicing microspherical $LiMn_{0.75}Fe_{0.25}PO_4$/C particles embedded in an epoxy resin with an ultramicrotome (UMT, MTX ultramicrotome, Tucson). The nitrogen adsorption-desorption isotherms (Autosorb-iQ 2ST/MP, Quantachrome) were measured at 77 K, and the surface area was calculated using the Brunauer-Emmett-Teller (BET) method. The pH values of the precursor and of the solution remaining after the end of reaction were recorded using a pH meter (Orion 3-star Benchtop Meter, Thermo Scientific). FTIR spectra (Vertex 70, Bruker) were obtained using KBr pellets. Inductively coupled plasma optical emission spectroscopy (ICP-OES) analysis (OPTIMA 7300DV, Perkin Elmer) was carried out to investigate the chemical composition of the $LiMn_{0.75}Fe_{0.25}PO_4$ powders. An elemental analyzer (2400 Series II CHNS/O, Perkin Elmer) was employed to determine the amount of carbon in the final products.

Electrochemical measurements

The working electrode was prepared by mixing 70 wt.% $LiMn_{0.75}Fe_{0.25}PO_4$/C microspheres, 20 wt.% acetylene black, and 10 wt.% polyvinylidene fluoride (PVDF; Aldrich) dissolved in *N*-methylpyrrolidone (NMP; Aldrich) as a binder. The slurry was coated on aluminum foil and dried in a vacuum oven at 100 °C for 24 h. The electrode was pressed with a roll-press machine. Each working electrode had an area of 1.13 cm^2 and the amount of active material in the electrode was 2 ~ 3 mg/cm^2. The electrochemical properties were investigated using CR2032 coin cells with lithium metal as the counter electrode. The electrolyte was 1 M $LiPF_6$ dissolved in a mixture of ethylene carbonate (EC)-ethyl methyl carbonate (EMC)-diethyl carbonate (DEC) at a volume ratio of 3:5:2. Cyclic voltammetry and galvanostatic charge/discharge tests were carried out between 2.0 and 4.5 V (vs. Li/Li^+) using a potentiostat/galvanostat (MPG2, Bio-Logic).

Results and discussion

Fig. 1a shows the XRD pattern of the $LiMn_{0.75}Fe_{0.25}PO_4$/C microspheres. All diffraction peaks of the $LiMn_{0.75}Fe_{0.25}PO_4$/C microspheres prepared at pH 6.35 correspond to those of orthorhombic olivine-structured materials with the *Pnma* space group (JCPDS card No. 74-0375).[1-3] Possible impurities such as lithium phosphate or metal phosphate were not detected in the XRD pattern, reflecting the high purity of the prepared sample. All diffraction peaks of $LiMn_{0.75}Fe_{0.25}PO_4$/C are significantly shifted to the right relative to those of $LiMnPO_4$, because the ionic radius of Fe^{2+} is smaller than that of Mn^{2+}.[3, 6] From the XRD data, the lattice constants of $LiMn_{0.75}Fe_{0.25}PO_4$/C microspheres were calculated to be a = 10.42 Å, b = 6.08 Å, c = 4.73 Å, and V = 299.70 $Å^3$, which are in good agreement with the lattice constants reported for phase-pure $LiMn_{0.75}Fe_{0.25}PO_4$.[6, 18] This means that the obtained $LiMn_{0.75}Fe_{0.25}PO_4$/C microspheres were a solid solution of $LiMnPO_4$ and $LiFePO_4$.

Fig. 1b shows FE-SEM image of the $LiMn_{0.75}Fe_{0.25}PO_4$/C microspheres. It can be seen that the $LiMn_{0.75}Fe_{0.25}PO_4$/C microspheres are composed of smaller primary particles with sizes of about 100 nm. The sizes of microspheres were uniform at about 2–3 μm. It is well known that a microspherical

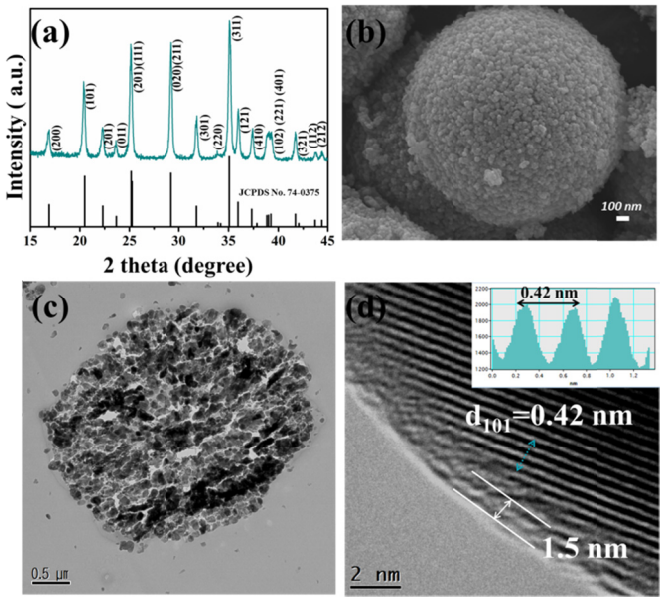

Fig. 1 (a) XRD pattern, (b) FE-SEM image, (c) cross-sectional TEM image, and (d) HR-TEM image of microsized spherical $LiMn_{0.75}Fe_{0.25}PO_4/C$.

morphology can help improve the tap density of the powder, because microspherical powders can be packed well.[24, 26] In fact, the $LiMn_{0.75}Fe_{0.25}PO_4/C$ microspheres have a high tap density of 1.3 g cm^{-3}, which is higher than the typical tap densities of nanoparticles of 0.3–0.8 g cm^{-3}. The high tap density of the microsized secondary particles helps to improve the volumetric capacity.[21] The EDS elemental mapping results for the $LiMn_{0.75}Fe_{0.25}PO_4/C$ microspheres are shown in Fig. S1. The Fe, Mn, C, P, and O species were uniformly distributed in the microspherical particles, and it is clear that the carbon was uniformly coated on the surfaces of the $LiMn_{0.75}Fe_{0.25}PO_4/C$ microspheres.

Fig. 1c shows a cross-sectional TEM image of a $LiMn_{0.75}Fe_{0.25}PO_4/C$ microsphere. It can be seen that the $LiMn_{0.75}Fe_{0.25}PO_4/C$ microspheres have a porous structure consisting of primary 50–100 nm nanoparticles and nanopores with diameters less than 50 nm. The nanosized primary particles create a network of nanopores that acts as a continuous pathway for the electrolyte ions to enter into the microsized materials, resulting in enhanced accessibility for Li ions throughout the structure. Fig. 1d shows an HR-TEM image of a $LiMn_{0.75}Fe_{0.25}PO_4/C$ microsphere. The HR-TEM image clearly shows a well-crystallized structure with lattice fringes of ca. 0.42 nm corresponding to the (101) interplanar spacing of the $LiMn_{0.75}Fe_{0.25}PO_4$.[6, 18] The thickness of the amorphous carbon layer on the surface of the $LiMn_{0.75}Fe_{0.25}PO_4/C$ microspheres was approximately 1.5–2 nm. The carbon content of the $LiMn_{0.75}Fe_{0.25}PO_4/C$ microspheres was measured to be 3 wt.% by elemental analysis (not shown here). The uniform and thin carbon coating improves the electrochemical performance of the $LiMn_{0.75}Fe_{0.25}PO_4/C$ microspheres.[28]

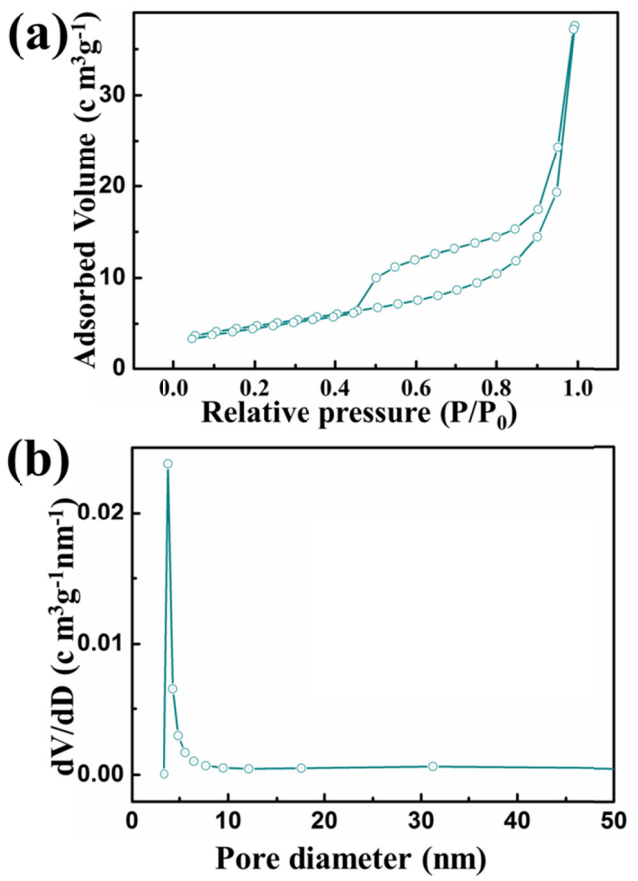

Fig. 2 (a) N_2 adsorption-desorption isotherms of microsized spherical $LiMn_{0.75}Fe_{0.25}PO_4/C$ and (b) the corresponding pore-size distribution calculated from the desorption branch using the BJH method.

Fig. 2 shows the nitrogen adsorption-desorption isotherms and the corresponding Barrett-Joyner-Halenda (BJH) pore-size distribution curve of the $LiMn_{0.75}Fe_{0.25}PO_4/C$ microspheres. It can be seen that the $LiMn_{0.75}Fe_{0.25}PO_4/C$ microspheres exhibit a typical type IV isotherm with a type H2 hysteresis loop, indicating a mesoporous structure. The specific surface area of the $LiMn_{0.75}Fe_{0.25}PO_4/C$ microspheres was 23.2 m^2 g^{-1}, which confirms the porous structure. As shown Fig. 2 (b), the mean pore size of the $LiMn_{0.75}Fe_{0.25}PO_4/C$ microspheres was 3.8 nm, and the distributions showed a uniform pore size with a sharp peak. The corresponding cumulative desorption volume of the pores is 0.06 cm^3 g^{-1}. These results support the conclusions about the porous structure derived from Fig. 1 c above.

In order to investigate the mechanism for the formation of the micro spherical $LiMn_{0.75}Fe_{0.25}PO_4/C$ particles, experiments were carefully carried out with different pH values of the precursor solution. Fig. 3 shows FE-SEM images of the samples prepared with precursors with different pH. The samples denoted as LMFP1, LMFP2, LMFP3, and LMFP4 were obtained from precursors with pH values of 5.74, 6.01, 6.35, and 7.89, respectively. As shown in Fig. 3a, LMFP1 has

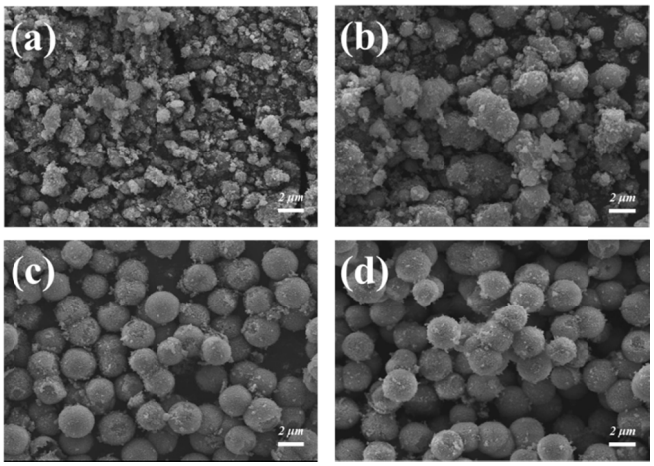

Fig. 3 FE-SEM images of $LiMn_{0.75}Fe_{0.25}PO_4/C$ prepared from precursors with different pH: (a) LMFP1, (b) LMFP2, (c) LMFP3, and (d) LMFP4.

an irregular morphology consisting of agglomerated nanoparticles. The LMFP2 shown in Fig. 3b are more spherical than the LMFP1. When the pH is increased to 6.35 and above, a surprising morphological change can be observed: LMFP3 and LMFP4 exhibit perfectly spherical morphologies, as shown in Fig. 3c and Fig. 3d. These spherical secondary particles are monodisperse, with a uniform size of about 2–3 μm. Thus, more microspherical morphologies were obtained in this synthesis system with increasing pH of the precursor, and we conclude that the pH of the precursor is a key factor affecting the resultant $LiMn_{0.75}Fe_{0.25}PO_4/C$ microspheres. Furthermore, time-dependent experiments at a fixed precursor pH of 6.35 proved that a more microspherical morphology is formed as time progresses in the microwave-assisted process, as shown in Fig. S2. To further gain insight into the effects of temperature on the formation of microspherical particles, different synthesis temperatures were used at a fixed precursor pH of 6.35. As shown in Fig. S3, the reaction temperature has no significant effect on the morphology of the product.

Based on the above experimental results, a possible mechanism for the formation of $LiMn_{0.75}Fe_{0.25}PO_4/C$ microspheres is proposed, as schematically illustrated in Fig. 4. It is well-known that the complexing agent acts as templates for synthesis of microspherical particles.[29, 30] In aqueous solution, citric acid has different properties depending on the pH.[31, 32] In particular, the pH has a critical role as deciding the oxidation state of the citrate ions $C_6H_{8-x}O_7^{x-}$: at low pH, the citric acid is not fully ionized and forms $[C_6H_7O_7^-]$ or $[C_6H_6O_7^{2-}]$, whereas at high pH, $[C_6H_5O_7^{3-}]$ is mostly formed as a result of full ionization.[31, 32] Therefore, when the pH of the precursor is increased, the electrostatic interactions between the citrate ions and metal ions are increased. At high pH, after the metal ion is uniformly bonded to $[C_6H_5O_7^{3-}]$, the $LiMn_{0.75}Fe_{0.25}PO_4$ precursor nuclei form homogeneously on all chelation sites on the citrate ions. These nuclei grow at the expense of smaller ones, following the Ostwald ripening process.[33] Then, the primary nanoparticles begin to assemble together to minimize the surface free energy of the system. Because citrate ions can form hydrogen bonds to each other, the primary particles grown from nuclei that were originally homogeneously distributed on the chelation sites of citrate ions at high pH can easily aggregate into microspherical secondary particles to minimize the surface energy.[34-36] Thus, uniform microspherical secondary particles are fabricated at high pH, because of the uniform distribution of the nuclei on the chelation sites of the citrate ions and the interactions between citrate ions. In contrast, at low pH, free metal ions exist in the solution, because the citric acid is not fully ionized. In this case, nuclei form randomly and are only partially bonded to citrate ions. As a result, self-assembly leads to secondary particles with irregular morphologies because of the weak interactions between the citrate ions and metal ions. Thus, whether $LiMn_{0.75}Fe_{0.25}PO_4/C$ microspheres form depends on the state of the citric acid at the chosen pH of the precursor.

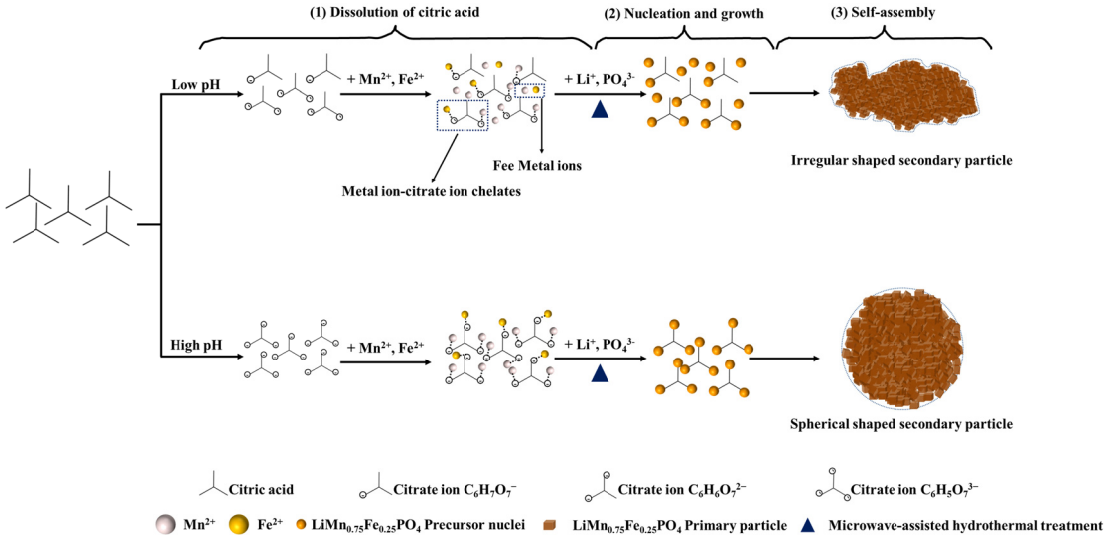

Fig. 4 Schematic illustration of the formation of $LiMn_{0.75}Fe_{0.25}PO_4$ microspheres.

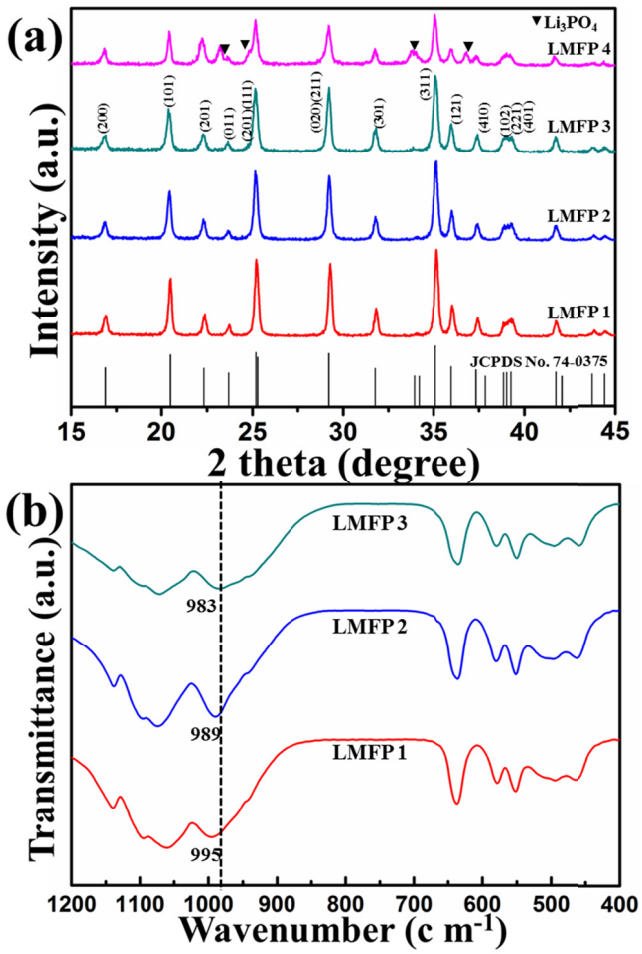

Fig. 5 (a) XRD patterns and (b) FT-IR spectra of $LiMn_{0.75}Fe_{0.25}PO_4/C$ prepared from precursors with different pH.

Fig. 5a shows the XRD patterns of the $LiMn_{0.75}Fe_{0.25}PO_4/C$ samples prepared at different pH. LMFP1, LMFP2, and LMFP3 (with precursor pH ≤ 6.35) maintained a single-phase olivine structure (JCPDS card No. 74-0375).[1-3] In the XRD pattern of LMFP4 (precursor pH = 7.89), small Li_3PO_4 peaks appeared at 23.2°, 24.8°, 33.8°, and 36.8°. It has been reported that Li_3PO_4 is generated at high pH because the solubility of Li_3PO_4 in basic solutions is very low.[37] Fig. 5b shows the FTIR spectra of LMFP1, LMFP2, and LMFP3, which do not contain Li_3PO_4, in the wavenumber range of 400–1200 cm^{-1}. The FTIR spectra in this range are widely used to determine the antisite defect concentrations in olivine-structured materials.[38] The FTIR spectra of the synthesized $LiMn_{0.75}Fe_{0.25}PO_4/C$ show the typical bands of olivine-structured materials reported elsewhere.[39] The vibration modes corresponding to the bands above 400 cm^{-1} are known to be external modes associated with the intramolecular vibrations of the PO_4 and MnO_6/FeO_6 units. The bands in the range of 500–580 cm^{-1} are known to correspond to the $(\nu_2+\nu_4)$ bending modes of $(PO_4)^{3-}$, and the band in the vicinity of 460 cm^{-1} is assumed to be a $(\nu_2+\nu_4)$ mode of $(PO_4)^{3-}$ involving lithium-ion motion. The band near ν_2 = 980 cm^{-1} is identified as the symmetric stretching mode. Bands related to the antisymmetric stretching mode of the P-O bond (ν_3) appear in the region of 1070–1139 cm^{-1}. The bands near 636 cm^{-1} are known to be bending modes of MnO_6/FeO_6 octahedrons.[40]

Table 1 Atomic ratios determined by ICP-OES analysis of $LiMn_{0.75}Fe_{0.25}PO_4/C$ prepared from precursors with different pH.

Sample	Li/P	Mn/P	Fe/P
LMFP1	0.90	0.74	0.26
LMFP2	0.97	0.74	0.26
LMFP3	1.00	0.75	0.25
LMFP4	1.03	0.73	0.27

In olivine-structured materials, the antisite defect is a defect in which a transition metal resides in the lithium site in the crystal lattice. Olivine-structured materials synthesized using the hydrothermal method intrinsically form $M_{Li}^{\bullet}$ (M = Mn, Fe) antisite defects.[41] These intrinsic antisite defects block the Li^+ migration channel and greatly degrade the electrochemical performance.[42, 43] As shown in Fig. 5b, the absorption band around 980 cm^{-1} of the samples shifts from 995 to 983 cm^{-1} with increasing precursor pH. This peak shift is related to a change in the antisite defect concentration.[38] In olivine-type $LiMn_{0.75}Fe_{0.25}PO_4/C$ material, the PO_4 tetrahedrons share edges or corners with MnO_6, FeO_6, and LiO_6 octahedrons. This indicates that the P-O bond in the PO_4 tetrahedron should be affected by changes in the surrounding MnO_6, FeO_6, and LiO_6 octahedrons. Therefore, $M_{Li}^{\bullet}$ (M = Mn, Fe) antisite defects may induce a change in the P-O bond in the PO_4 tetrahedrons, resulting in a shift in the vibration frequencies. The blue shift of the above peak is known to reflect a reduction in the antisite defect concentration.[38] As a result, it is reasonable to conclude that the $M_{Li}^{\bullet}$ (M = Mn, Fe) antisite defect concentration of the hydrothermally synthesized $LiMn_{0.75}Fe_{0.25}PO_4/C$ decreases as the precursor pH increases.

To verify the chemical formula of the $LiMn_{0.75}Fe_{0.25}PO_4/C$, the Li/P, Mn/P, and Fe/P atomic ratios of each sample were measured by ICP-OES analysis, as shown in Table 1. The Mn/P and Fe/P atomic ratios were similar for all samples, in the ranges of 0.73–0.75 and 0.24–0.27, respectively. However, the Li/P atomic ratio increased from 0.90 to 1.03 with increasing precursor pH. The Li/P atomic ratios for LMFP1, LMFP2, and LMFP3 gradually increased to 1. These results are consistent with the FTIR spectra in suggesting that the concentration of $M_{Li}^{\bullet}$ (M = Mn, Fe) antisite defects decreases with increasing precursor pH. As mentioned above, the Li/P atomic ratios (Mn/P+Fe/P) for LMFP3 were close to 1, which is thought to be obtained near the equilibrium state, and LMFP3 showed a single-phase olivine structure without any impurities. In contrast, the Li/P atomic ratio for LMFP4 was significantly higher because it contains Li_3PO_4 impurities. Finally, ICP-OES analysis of the products revealed that the Li/P, Mn/P, and Fe/P

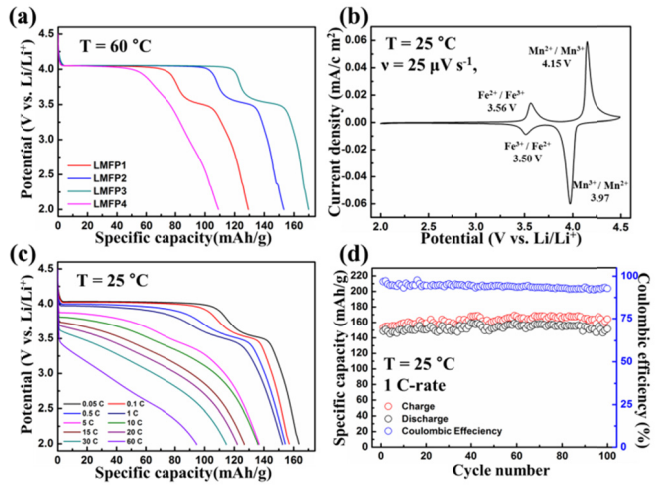

Fig. 6 (a) Galvanostatic discharge curves of $LiMn_{0.75}Fe_{0.25}PO_4/C$ prepared from precursors with different pH measured at 60 °C. The cells were charged at 0.05 C-rate to 4.5 C, kept at 4.5 V until the limit current 0.01 C-rate was reached, and then discharged at 0.05 C-rate to 2.0 V. (b) Cyclic voltammogram (CV) of $LiMn_{0.75}Fe_{0.25}PO_4/C$ microspheres (LMFP3) obtained at scan rate of 0.025 mV s^{-1} measured at 25°C. (c) Galvanostatic discharge curves of $LiMn_{0.75}Fe_{0.25}PO_4/C$ microspheres (LMFP3) obtained at different current rates at 25°C. The cells were charged at different current rates to 4.5 V, kept at 4.5 V until the limit current 0.01 C-rate was reached, and then discharged at different current rates to 2.0 V. (d) Cyclability of $LiMn_{0.75}Fe_{0.25}PO_4/C$ microspheres (LMFP3) at 1 C-rate over 100 cycles.

atomic ratios of LMFP3 (weakly acidic precursor) are close to the chemical formula of $LiMn_{0.75}Fe_{0.25}PO_4/C$.

Fig. 6a shows the galvanostatic discharge curves of the samples for a charge/discharge current of 0.05 C-rate measured at 60 °C. The discharge capacities of LMFP1 and LMFP2 were 129 mAh g^{-1} and 153 mAh g^{-1}, respectively. Because LMFP1 and LMFP2 had higher concentrations of $M_{Li}^{\cdot}$ (M = Mn, Fe) antisite defects than LMFP3, their discharge capacities were much lower. LMFP3 showed the highest discharge capacity of 170 mAh g^{-1}, which corresponded to 99.4% of the theoretical capacity. This could be attributed to the low concentration of antisite defects and the porous structure, which allowed the electrolyte to easily be absorbed into the inner parts of the microspheres. The discharge capacity of the LMFP4 synthesized under weak basic conditions was much lower, 109 mAh g^{-1}, because of the Li_3PO_4 impurity, as shown in Fig 5a. Li_3PO_4 has been reported to severely degrade electrochemical performance.[37]

Fig. 6b shows cyclic voltammograms (CVs) for LMFP3, which delivered the largest discharge capacity in Fig. 6a, taken at a potential scan rate of 0.025 mV s^{-1} in the potential window of 2.0–4.5 V at 25 °C. The CV at 0.025 mV s^{-1} clearly shows two sets of current peaks at 4.15 V/3.97 V and 3.56 V/3.50 V, which correspond to phase-pure $LiMn_{0.75}Fe_{0.25}PO_4/C$.[6, 44] The CVs of LMFP3 obtained at scan rates of 0.025, 0.05, 0.1, 0.2, 0.5, and 1 mV s^{-1} are shown in Fig. S4. Interestingly, the shape of the CV was well maintained, even when the potential scan rate was increased up to 1 mV s^{-1}. This result suggests the good high rate capability of LMFP3.[45-48]

The charge-discharge curves of LMFP3 at 0.05 C-rate measured at 25 °C are shown in Fig. S5. The charge and discharge capacities of LMFP3 were found to be 168 mAh g^{-1} and 163 mAh g^{-1} at 0.05 C-rate, respectively, which corresponds to 95.3% of the theoretical capacity. The coulombic efficiency (calculated from the discharge capacity/charge capacity) was about 97 %. In addition, the discharge capacity in terms of the volumetric capacity at 0.05 C-rate is 262 mAh cm^{-3}, which is similar the reported value.[26] Fig. 6c shows the discharge curves of LMFP3 obtained between 2.0 and 4.5 V (vs. Li/Li^+) at 0.05 to 60 C-rates, measured with a half-cell system using coin cell at 25 °C. It should be noted that the charge and discharge tests were performed at the same C-rates. The discharge capacity measured at the extremely high 60 C-rate was about 100 mAh g^{-1}, which is 57% of the specific capacity at 0.05 C-rate, indicating the excellent high-rate capability of the prepared $LiMn_{0.75}Fe_{0.25}PO_4/C$ microspheres (Fig. S6). In addition, the coulombic efficiency at the extremely high 60 C-rate was about 90 % (Fig. S7). This could be attributed to the uniform carbon coating on the surface of $LiMn_{0.75}Fe_{0.25}PO_4/C$ microspheres, which effectively reduced the charge transfer resistance. Furthermore, the porous spherical structure of the $LiMn_{0.75}Fe_{0.25}PO_4/C$ microspheres ensures deep penetration of the electrolyte into inner parts of micro spherical secondary particles, enabling full electrochemical utilization of the $LiMn_{0.75}Fe_{0.25}PO_4/C$ microspheres.

Fig. 6d shows the cycling stability of LMFP3. The cycling test was conducted at 25 °C for 100 cycles at a charge/discharge rate of 1 C-rate. The initial discharge capacity was 152 mAh g^{-1}. After 100 cycles, LMFP3 delivered a discharge capacity of 151 mAh g^{-1}, which corresponds to 99.3% capacity retention. In addition, the coulombic efficiency remained at about 96 %, demonstrating the excellent cyclability of LMFP3. This indicates the excellent structural stability of LMFP3 during repeated cycling.

Conclusion

In summary, $LiMn_{0.75}Fe_{0.25}PO_4/C$ microspheres were synthesized using a facile and simple microwave-assisted process with a complexing agent. It was found that the different states of the complexing agent for different pH of the precursor solution have significant effects on the obtained microspherical morphology and the electrochemical performance. The obtained microspherical secondary particles were composed of nanosized primary particles. The $LiMn_{0.75}Fe_{0.25}PO_4/C$ microspheres exhibited a high tap density of 1.3 g cm^{-3}, a reversible capacity of 163 mAh g^{-1} at a 0.05 C-rate, and remarkable rate capability, with 57% capacity retention at a 60 C-rate. In addition, excellent cyclability was observed, with 99.3% capacity retention after 100 cycles at 1 C-rate. These superior properties could be attributed to the porous spherical structure, uniform carbon coating layer, and the reduction of the antisite defect concentration.

Acknowledgements

This work was supported by the energy efficiency and resources of the Korea Institute of Energy Technology Evaluation and Planning (KETEP) grant funded by the Ministry of Knowledge Economy, Korean government (No: 20122010100140), and also supported by POSCO.

Notes and references

a Department of Material Science and Engineering, Yonsei University, 134 Shinchon-dong, Seodaemoon-gu, Seoul 120-749, Republic of Korea. Fax: +82-2-312-5375; Tel: +82-2-365-7745; E-mail: kbkim@yonsei.ac.kr.
b Energy Efficient Materials Team, Energy & Environmental Division, Korea Institute of Ceramic Engineering & Technology, 233-5 Gasan-dong, Guemcheon-gu, Seoul 153-801, Republic of Korea. Fax: +82-2-3282-2475; Tel: +82-2-3282-2463; E-mail: rkc@kicet.re.kr.

† Electronic Supplementary Information (ESI) available: one table and eight figures showing further details of the properties of the $LiMn_{0.75}Fe_{0.25}PO_4$/C microspheres. See DOI: 10.1039/c000000x/

1. A. K. Padhi, K. S. Nanjundaswamy and J. B. Goodenough, *J Electrochem Soc*, 1997, 144, 1188-1194.
2. S. F. Yang, P. Y. Zavalij and M. S. Whittingham, *Electrochem Commun*, 2001, 3, 505-508.
3. A. Yamada and S. C. Chung, *J Electrochem Soc*, 2001, 148, A960-A967.
4. C. Delacourt, P. Poizot, M. Morcrette, J. M. Tarascon and C. Masquelier, *Chem Mater*, 2004, 16, 93-99.
5. G. H. Li, H. Azuma and M. Tohda, *Electrochem Solid St*, 2002, 5, A135-A137.
6. S. K. Martha, J. Grinblat, O. Haik, E. Zinigrad, T. Drezen, J. H. Miners, I. Exnar, A. Kay, B. Markovsky and D. Aurbach, *Angew Chem Int Edit*, 2009, 48, 8559-8563.
7. A. Yamada, Y. Kudo and K. Y. Liu, *J Electrochem Soc*, 2001, 148, A747-A754.
8. M. Yonemura, A. Yamada, Y. Takei, N. Sonoyama and R. Kanno, *J Electrochem Soc*, 2004, 151, A1352-A1356.
9. C. Delacourt, L. Laffont, R. Bouchet, C. Wurm, J. B. Leriche, M. Morcrette, J. M. Tarascon and C. Masquelier, *J Electrochem Soc*, 2005, 152, A913-A921.
10. D. Morgan, A. Van der Ven and G. Ceder, *Electrochem Solid St*, 2004, 7, A30-A32.
11. D. W. Choi, D. H. Wang, I. T. Bae, J. Xiao, Z. M. Nie, W. Wang, V. V. Viswanathan, Y. J. Lee, J. G. Zhang, G. L. Graff, Z. G. Yang and J. Liu, *Nano Lett*, 2010, 10, 2799-2805.
12. S. L. Shang, Y. Wang, Z. G. Mei, X. D. Hui and Z. K. Liu, *Journal of Materials Chemistry*, 2012, 22, 1142-1149.
13. A. Yamada, Y. Kudo and K. Y. Liu, *J Electrochem Soc*, 2001, 148, A1153-A1158.
14. A. Yamada, Y. Takei, H. Koizumi, N. Sonoyama, R. Kanno, K. Itoh, M. Yonemura and T. Kamiyama, *Chem Mater*, 2006, 18, 804-813.
15. J. Molenda, W. Qjczyk and J. Marzec, *Journal of Power Sources*, 2007, 174, 689-694.
16. Z. Tan, P. Gao, F. Q. Cheng, H. J. Luo, J. T. Chen, H. H. Zhou and S. T. Tan, *Funct Mater Lett*, 2011, 4, 299-303.
17. S. M. Oh, H. G. Jung, C. S. Yoon, S. T. Myung, Z. H. Chen, K. Amine and Y. K. Sun, *Journal of Power Sources*, 2011, 196, 6924-6928.
18. K. Saravanan, V. Ramar, P. Balaya and J. J. Vittal, *Journal of Materials Chemistry*, 2011, 21, 14925-14935.
19. H. L. Wang, Y. Yang, Y. Y. Liang, L. F. Cui, H. S. Casalongue, Y. G. Li, G. S. Hong, Y. Cui and H. J. Dai, *Angew Chem Int Edit*, 2011, 50, 7364-7368.
20. Z. H. Chen and J. R. Dahn, *J Electrochem Soc*, 2002, 149, A1184-A1189.
21. Y. G. Wang, P. He and H. S. Zhou, *Energ Environ Sci*, 2011, 4, 805-817.
22. J. F. Qian, M. Zhou, Y. L. Cao, X. P. Ai and H. X. Yang, *J Phys Chem C*, 2010, 114, 3477-3482.
23. S. M. Oh, S. T. Myung, Y. S. Choi, K. H. Oh and Y. K. Sun, *Journal of Materials Chemistry*, 2011, 21, 19368-19374.
24. Y. K. Sun, S. M. Oh, H. K. Park and B. Scrosati, *Advanced materials*, 2011, 23, 5050-5054.
25. S. M. Oh, S. T. Myung, J. B. Park, B. Scrosati, K. Amine and Y. K. Sun, *Angew Chem Int Edit*, 2012, 51, 1853-1856.
26. W. Liu, P. Gao, Y. Y. Mi, J. T. Chen, H. H. Zhou and X. X. Zhang, *Journal of Materials Chemistry A*, 2013, 1, 2411-2417.
27. M. Y. Cho, K. B. Kim, J. W. Lee, H. Kim, H. Kim, K. Kang and K. C. Roh, *Rsc Adv*, 2013, 3, 3421-3427.
28. J. Moskon, R. Dominko, R. Cerc-Korosec, M. Gaberscek and J. Jamnik, *Journal of Power Sources*, 2007, 174, 683-688.
29. F. Yu, J. J. Zhang, Y. F. Yang and G. Z. Song, *Journal of Power Sources*, 2009, 189, 794-797.
30. S. Cho, J. W. Jang, S. H. Jung, B. R. Lee, E. Oh and K. H. Lee, *Langmuir*, 2009, 25, 3825-3831.
31. A. Loewenstein and J. Roberts, *J. Am. Chem. Soc.*, 1960, 82, 2705-2710.
32. R. N. Goldberg, N. Kishore and R. M. Lennen, *J Phys Chem Ref Data*, 2002, 31, 231-370.
33. W. Z. Ostwald, *Phys. Chem*, 1900, 34, 495-503.
34. M. Ocana, R. Rodriguezclemente and C. J. Serna, *Advanced materials*, 1995, 7, 212-216.
35. L. Xu, C. L. Lu, Z. H. Zhang, X. Y. Yang and W. H. Hou, *Nanoscale*, 2010, 2, 995-1005.
36. J. Su, X. L. Wu, C. P. Yang, J. S. Lee, J. Kim and Y. G. Guo, *J Phys Chem C*, 2012, 116, 5019-5024.
37. K. Dokko, S. Koizumi, H. Nakano and K. Kanamura, *Journal of Materials Chemistry*, 2007, 17, 4803-4810.
38. X. Qin, J. M. Wang, J. Xie, F. Z. Li, L. Wen and X. H. Wang, *Phys Chem Chem Phys*, 2012, 14, 2669-2677.
39. F. Brochu, A. Guerfi, J. Trottier, M. Kopec, A. Mauger, H. Groult, C. M. Julien and K. Zaghib, *Journal of Power Sources*, 2012, 214, 1-6.
40. C. M. Burba and R. Frech, *J Electrochem Soc*, 2004, 151, A1032-A1038.
41. J. J. Chen, M. J. Vacchio, S. J. Wang, N. Chernova, P. Y. Zavalij and M. S. Whittingham, *Solid State Ionics*, 2008, 178, 1676-1693.
42. G. R. Gardiner and M. S. Islam, *Chem Mater*, 2010, 22, 1242-1248.
43. R. Malik, D. Burch, M. Bazant and G. Ceder, *Nano Lett*, 2010, 10, 4123-4127.
44. V. Ramar and P. Balaya, *Phys Chem Chem Phys*, 2013, 15, 17240-17249.

45. S. M. Bak, K. W. Nam, C. W. Lee, K. H. Kim, H. C. Jung, X. Q. Yang and K. B. Kim, *Journal of Materials Chemistry*, 2011, 21, 17309-17315.
46. J. P. Jegal and K. B. Kim, *Journal of Power Sources*, 2013, 243, 859-864.
47. H. K. Kim, J. P. Jegal, J. Y. Kim, S. B. Yoon, K. C. Roh and K. B. Kim, *Journal of Materials Chemistry A*, 2013, 1, 14849-14852.
48. H. K. Kim, K. C. Roh, K. Kang and K. B. Kim, *Rsc Adv*, 2013, 3, 14267-14272.

Synthesis of $LiMn_{0.75}Fe_{0.25}PO_4/C$ microspheres using a microwave-assisted process with a complexing agent for high-rate lithium ion batteries

Myeong-Seong Kim[a], Jong-Pil Jegal[a], Kwang Chul Roh[*b] and Kwang-Bum Kim[*a]

[a] *Department of Materials Science & Engineering, Yonsei University, 50 Yonsei-ro, Seodaemun-gu, Seoul 120-749, Republic of Korea. E-mail: kbkim@yonsei.ac.kr*

[b] *Energy Efficient Materials Team, Energy & Environmental Division, Korea Institute of Ceramic Engineering & Technology, 233-5 Gasan-dong, Guemcheon-gu, Seoul 153-801, Republic of Korea. E-mail: rkc@kicet.re.kr*

Table of contents entry

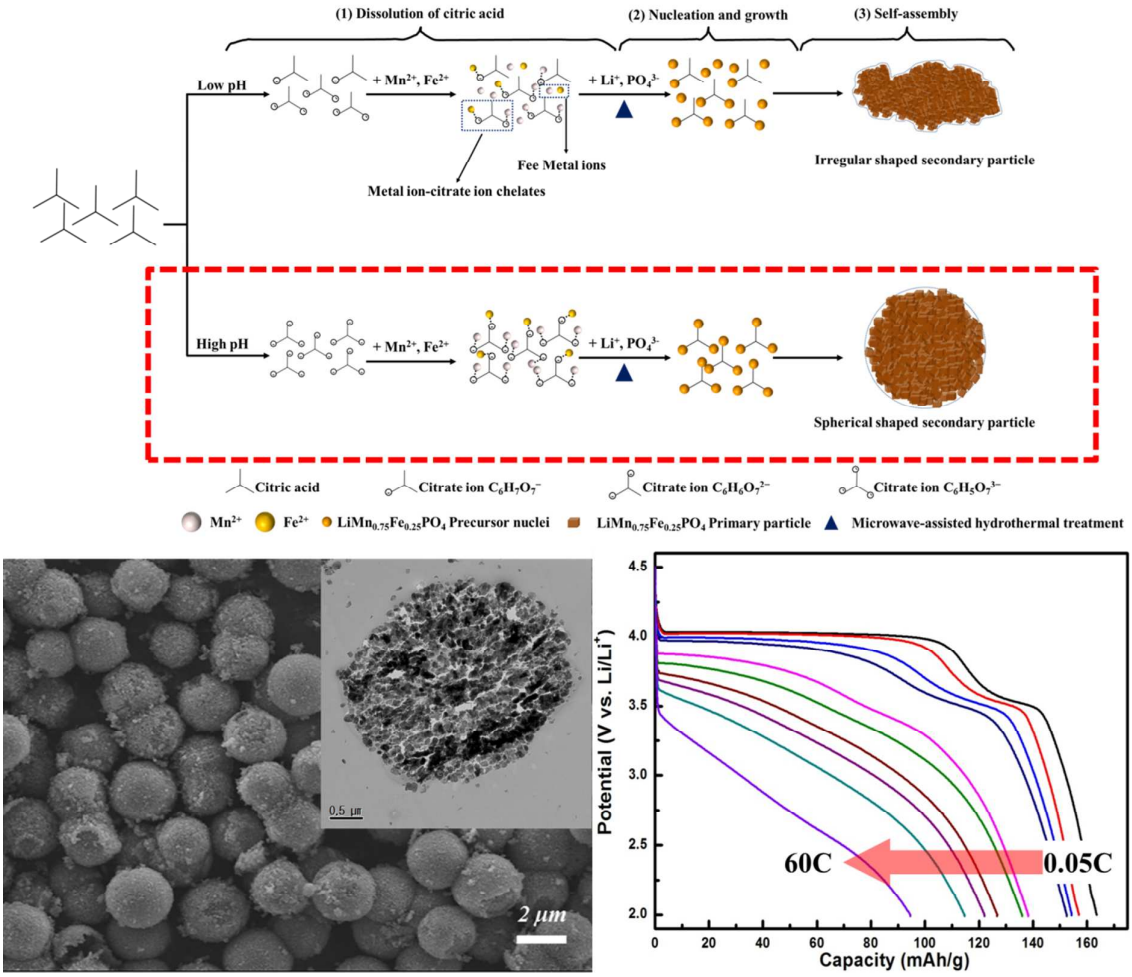

$LiMn_{0.75}Fe_{0.25}PO_4/C$ microspheres were synthesized using a microwave-assisted process with a complexing agent through the control of precursor pH. The prepared secondary spheres have a high tap density of 1.3 g cm^{-3} and deliver a reversible capacity of 163 mAh g^{-1} at a 0.05 C-rate. Furthermore, remarkable rate capability is obtained, with 57% capacity retention at a 60 C-rate, as well as excellent cyclability, with 99.3% capacity retention after 100 cycles at 1 C-rate. These superior properties could be attributed to the porous spherical structure, uniform carbon coating layer, and the reduction of the antisite defect concentration.